Analysis and Modeling of Spectral Line Shapes of Collision-Induced Light Scattering of Gaseous Xenon

Jean-Luc Godet, M. S. A. El-Kader

Analysis and modeling of spectral line shapes of collision-induced light scattering of gaseous xenon

J.-L. Godet [a*], M.S.A. El-Kader [b*],

[a] *Laboratoire de photonique d'Angers (LPHIA), Université d'Angers, 2 boulevard Lavoisier, 49045 Angers, France*

[b] *Department of Engineering Mathematics and Physics, Faculty of Engineering, Cairo University, Giza, 12211, Egypt*

Keywords

Xenon, Interatomic potential, CILS, Pair polarizability,

Abstract

Collision-induced light scattering spectra of gaseous xenon at room temperature are analyzed in terms of different literature and new interatomic potentials and interaction-induced pair polarizability anisotropy and trace models. At low frequencies the spectral intensities and the associated moments are determined by both bound and free transitions. The spectra at intermediate and high frequencies are sensitive to both the attractive part of the potential and to short-range values of the anisotropy or trace polarizability. An empirical interatomic potential for the gaseous xenon interaction is developed by simultaneously fitting the Barker et al. (BFW) and modified Tang-Toennies (MTT) potentials to spectroscopic and thermal properties over a wide temperature range. The quality of the present potentials was checked by comparison between the calculated and experimental transport properties at different temperatures. The results show that these are the most accurate potentials reported to date for xenon gas. Similarly, the combination of these potentials with our analytical models of xenon polarizability is satisfactory for both the reproduction of spectral moments and spectral line shapes of the xenon collision-induced spectra.

doi.org/10.36959/562/617

*Corresponding author.

E-mail addresses: jean-luc.godet@univ-angers.fr (J.-L. Godet), mohamedsay68@eng.cu.edu.eg (M.S.A. El-Kader)

1. Introduction

The collision-induced light scattering (CILS) spectrum of two atoms or molecules is shaped by two functions of their separation r: the interaction potential and the induced polarizability tensor of the atom or molecule pair. In the case of a noble gas like xenon, the interaction potential V can, to a first approximation, be considered isotropic; it depends only on r. Moreover, the knowledge of the polarizability tensor is summarized by that of its trace $\alpha(r)$ and its anisotropy $\beta(r)$ [1]. The theoretical challenge is thus to determine the potential, the trace and the anisotropy which reproduce by calculation what can be measured experimentally. The spectra of xenon have been measured in the past [2, 3] and more recently [4, 5] by several groups which have given consistent results, both for spectra related to the anisotropy of the polarizability tensor and for that specifically related to its trace. Early studies [2, 3] used empirical models of polarizability. The group of Chrysos [4, 5] used the relatively recent ab initio calculations of the xenon trace and anisotropy by Maroulis et al. [6]. However, the interatomic potentials used by all these groups for their theoretical calculations were empirical and quite old [7, 8]. In this paper, we propose two new potentials based on different sets of experimental measurements. Similarly, we propose analytical models of the anisotropy and trace of xenon based on the analysis of CIS spectral moments. These semi-empirical models, insofar as they allow to reproduce well what is observed experimentally, can be a useful reference for any ab initio calculation of the potential or the polarizability of xenon.

No accurate potential is available to fit the different properties for xenon. We calculate an approximate interatomic potential for the xenon interaction using mostly the methods outlined in previous papers [9–11]. Since the details of the methods are given there and the references therein, we will only restate the equations when it is necessary for the sake of continuity. To reiterate, the basic strategy in this paper is to include spectroscopic properties, thermo-physical and transport properties in addition to the data of collision induced light scattering data (CILS) to fit the Barker, Fisher and Watts (BFW) and Modified Tang-Toennies (MTT) potential models for interatomic xenon interactions. Different experiments are sensitive to different regions of the interatomic potential. The pressure virial coefficients reflect the size of r_m and the volume of the attractive well [12]. The viscosity, self-diffusion, thermal conductivity and thermal diffusion factors data are most sensitive to the wall of the potential from r_m inward to a point where the potential is repulsive [13]. Collision-induced light scattering (CILS) intensities are most sensitive to the attractive potential from r_m at which the potential has its minimum out to the asymptotic long range region, and the rainbow and supernumerary oscillations give detailed information about that part of the potential [14]. Thus, these six properties with the spectroscopic data can, in principle, be used to develop a potential over a fairly broad range of interatomic distances.

Our paper is organized as follows: our two interatomic potential models are presented in section 2 along with the multi-property analysis that allowed us to determine their parameters. After a brief

presentation of collision-induced light scattering, section 3 is devoted to depolarized and isotropic spectra of xenon, calculated for different potentials and different anisotropy and trace models, including the analytical models we determined and propose. Concluding remarks are given in Section 4.

2. Multi-property analysis and the interatomic potentials of Xenon

The interatomic potentials we provide here are obtained through the analysis of the vibrational energy levels [15-22], pressure second virial coefficients [23-35] and a set of gaseous transport properties [36-52]. For the analysis of all these experimental data we consider the following potentials

A- BFW potential

The empirical Barker, Fisher and Watts (BFW) interatomic potential [53] is represented by the following formula

$$V(r)=\varepsilon\sum_{i=0}^{5}A_i\left(x-1\right)^i\exp\left(\xi\left(1-x\right)\right)-\sum_{n=3}^{\infty}\frac{C_{2n}}{x^{2n}+\zeta} \tag{1}$$

where $x=r/r_m$ is the reduced distance, ε is the potential depth, r_m is the distance at the minimum potential and the rest (ξ, ζ) are fitting parameters.

B- MTT potential

The modified Tang-Toennies model (MTT) which in the whole range of interactions can be represented by the formula [54]

$$V(r)=Ar^{\left(\frac{7}{2\mathfrak{B}}-1\right)}\exp\left(-2\mathfrak{B}r\right)-\sum_{n=3}^{\infty}\frac{C_{2n}\,f_{2n}(r)}{r^{2n}} \tag{2}$$

where $f_{2n}(r)$ is the appropriate damping functions, given by the expression derived by Tang and Toennies [55]

$$f_{2n}(r)=1-\exp\left(-b(r)\right)\sum_{k=0}^{2n}\frac{[b(r)]^k}{k!} \tag{3}$$

and

$$b(r)=1-\frac{7}{2\mathfrak{B}}+2\mathfrak{B}\,r \tag{4}$$

Even at the present (BFW) level, there are really thirteen parameters (ε, r_m, A_0, A_1, A_2, A_3, A_4, A_5, ξ, ζ, C_6, C_8, C_{10}) and in the (MTT) level, there are seven free parameters (ε, r_m, A, $\mathfrak{B}$, C_6, C_8, C_{10}) which are far too many to determine from the present data. Accordingly we proceeded as follows: the coefficients A_0, A_1, A and $\mathfrak{B}$ are determined from the conditions of continuity. The long-range dispersion coefficients C_6, C_8, C_{10} were taken from theoretical calculations of Thakkar et al. [56], leaving rest parameters in these

models that were varied to fit the vibrational energy levels V. This minimization is further supported by calculating δ_B, δ_η, δ_λ, δ_D, and δ_α, the rms deviations calculated from second pressure virial coefficients, viscosity, thermal conductivity, diffusion coefficients and thermal diffusion factor, respectively. This decision leads to the potentials parameters in Table 1 as our best estimate of Xe_2 interatomic potentials.

Table 1. Parameters of the different interatomic potentials and the associated values of δ.

For xenon interaction, ζ=0.01. Besides, δ_j is defined by $\delta_j^2 = \frac{1}{n_j}\sum_{i=1}^{n_j}\Delta_{ji}^{-2}\left(P_{ji} - p_{ji}\right)^2$,

where P_{ji} and p_{ji} are, respectively, the calculated and experimental values of property j at point i and Δ_{ji} is the experimental uncertainty of property j at point i. The subscripts V, B, η, λ, D, and α_{iso} refer to the vibrational energy levels, interaction second pressure virial coefficient, viscosity, thermal conductivity, diffusion coefficient and thermal diffusion factor, respectively.

The overall rms deviation was obtained from $\delta_\circ = \sqrt{\frac{1}{N}\sum_{j=1}^{N}\delta_j^2}$.

Pots.	ε/k_B (T)	r_m (Å)	ξ	A_0	A_1	A_2	A_3	A_4	A_5	A	B
BFW	283.0	4.37	14.75	1.05039	0.352462	−2.60148	−8.0	21.0	54.0		
MTT	284.0	4.368								80.0168	1.00908

Pots.	δ_V	δ_B	δ_η	δ_λ	δ_D	δ_{iso}	$\delta_\circ$
BFW	0.75	0.86	0.62	0.59	0.87	0.93	0.78
MTT	0.77	0.89	0.66	0.63	0.91	0.97	0.82

2.1. Vibrational Energy Spacings

With the above obtained interaction potentials the vibrational energy spacings can be calculated by solving the radial one-dimensional Schrödinger equation. In the present paper this equation is solved numerically. The interaction potentials of homonuclear and heteronuclear rare-gas dimers with the internuclear separation between 3.0 a.u. and 200 a.u. are used to do the calculation. The size of the grid points is 1600. Table 2 presents the calculation results for Xe_2 dimers. It is seen from Table 2 that the agreement of the two sets of spacings predicted by the MTT and BFW is good.

The experimental and other theoretical results are also listed in the Table 2 for comparison [15-22]. It is gratifying to find that the spacings of these dimers predicted by the MTT and BFW potential models are in excellent agreement with the experimental results if the experimental error bar are taken into consideration.

Table 2: Comparison of our computed vibrational energy spacings for Xe_2 gas with experimental and other theoretical data. All values are given in cm^{-1}.

	BFW	MTT	Sheng [15]	Xie [16]	Hellmann [17]	Aziz [18]	Dham [19]	Slavíček [20]	Hanni [21]	Lit.results [22]
0-1	19.67	20.02	19.369	19.5	19.31±0.08	19.61	19.61	18.69	19.39	19.90±0.3
1-2	18.47	18.75	18.214	18.37	18.15±0.08	18.41	18.45	17.53	18.23	18.55±0.3
2-3	17.27	17.49	17.06	17.23	16.99±0.09	17.21	17.28	16.37	17.08	17.20±0.3
3-4	16.08	16.24	15.92	16.08	15.83±0.09	16.02	16.09	15.21	15.93	16.17±0.3
4-5	14.90	14.99	14.81	14.93	14.68±0.09	14.83	14.89	14.07	14.79	14.63±0.3
5-6	13.71	13.77	13.65	13.78	13.54±0.09	13.66	13.71	12.92	13.65	13.70±0.3
6-7	12.54	12.57	12.34	12.62	12.41±0.09	12.50	12.54	11.79	12.52	12.63±0.3
7-8	11.39	11.39	11.11	11.48	11.29±0.09	11.35	11.40	10.68	11.41	11.33±0.3
8-9	10.26	10.23	10.28	10.35	10.19±0.09	10.23	10.27	9.58	10.32	10.15±0.3
9-10	9.16	9.11	9.604	9.24	9.12±0.09	9.14	9.16	8.51	9.25	8.95±0.3

2.2. Analysis of second pressure virial coefficients

An effective means for checking the validity of the different potential parameters can be made using second pressure virial coefficient data [23-35] at different temperatures. The interaction second pressure virial coefficient B at temperature T was calculated classically with the first three quantum corrections from [57]:

$$\mathrm{B}(T) = \mathrm{B}_{\mathrm{cl}}(T) + \lambda \mathrm{B}_{\mathrm{qm},1}(T) + \lambda^2 \mathrm{B}_{\mathrm{qm},2}(T) + +\lambda^3 \mathrm{B}_{\mathrm{qm},3}(T) \tag{5}$$

where

$$\mathrm{B}_{\mathrm{cl}}(T) = 2\pi N_0 \int_0^{\infty} \left[1 - \exp\left(-\frac{V(r)}{k_B T} \right) \right] r^2 dr \tag{6}$$

with $\lambda=\hbar^2/(12mk_BT)$, $\hbar=h/2\pi$. m and N_0 are the atomic mass and Avogadro's number. The first three quantum corrections $\mathrm{B}_{\mathrm{qm},1}(T)$, $\mathrm{B}_{\mathrm{qm},2}(T)$ and $\mathrm{B}_{\mathrm{qm},3}(T)$, are given in Ref.[57].

The calculated B_{12} was compared with the experimental results [23-35] using the present BFW intermolecular potentials. As it may be clearly seen in Fig.1 and Table 1, the interatomic BFW and MTT potentials give the best agreement with the experimental values over a high range of temperatures.

2.3. Analysis of traditional transport properties

An additional check on the proposed potential consists of the calculation of the transport properties i.e. viscosity $\eta(T)$, diffusion coefficient $D(T)$, thermal conductivity $\lambda(T)$ and isotopic thermal factor $\alpha_{\mathrm{iso}}(T)$ at different temperatures T of xenon. These are obtained via the formulae of Monchick *et. al* [58] and their comparison to the accurate experimental and theoretical results [36-52] which are clear by calculating the

associated values of δ_j as shown in Table 1. The agreements for system under consideration are excellent

in the whole temperature range.

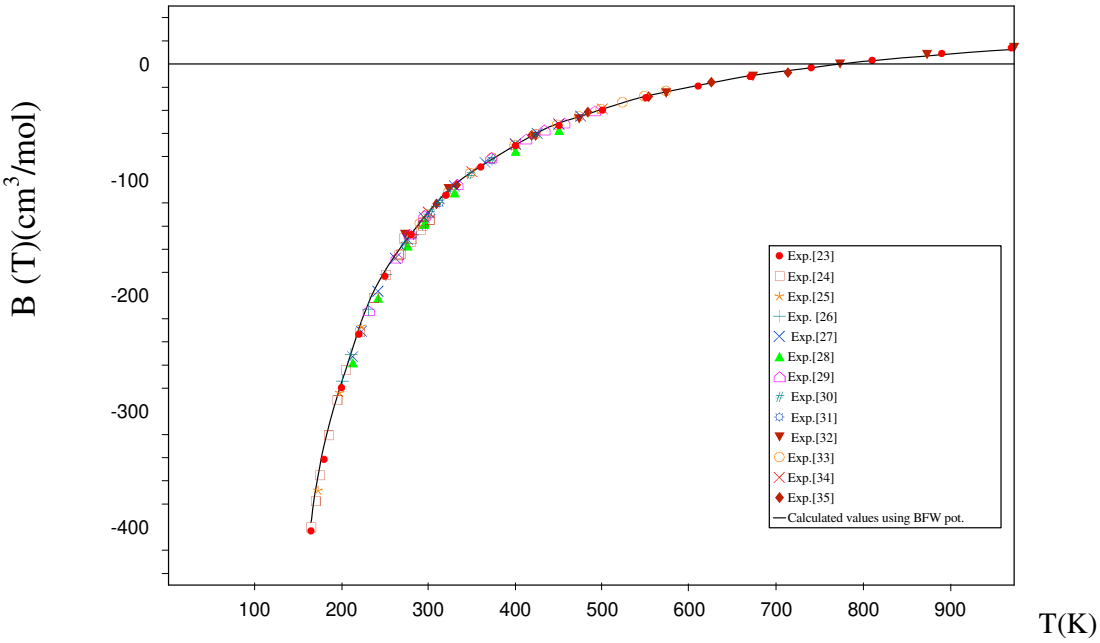

Fig.1. Temperature dependence of the xenon gas interaction pressure second virial coefficients B in $cm^3\ mol^{-1}$ versus temperature in K. Comparison is made with previously available experimental and theoretical results [23-35]. The Calculations were performed using the present BFW interatomic potential.

3. Application to the calculation of light scattering spectra

3.1. Principles of CILS spectrum calculations

In a gas of atoms or molecules excited by a laser line of wavelength λ_L, a light scattering spectrum is observable on both sides of the Rayleigh line, the origin of which can be attributed to collision-induced (CI) interactions. By studying this spectrum at different pressures, it is possible to extract its part proportional to the square of the density due to binary interactions [59]. Moreover, the incident laser beam can be polarized parallel (//) or perpendicular ($\perp$) to the scattering plane. Two binary spectra can therefore be distinguished: the "depolarized" collision-induced light scattering (CILS) spectrum $I_{//}(\nu)$ and the "polarized" spectrum $I_{\perp}(\nu)$, where ν stands for the frequency shift relative to $\nu_L=c/\lambda_L$. In a typical 90° scattering experiment, these two experimental spectra can be expressed in terms of the isotropic[1]

[1] The isotropic spectrum is called "polarized" spectrum in some books or papers; we do not adopt this characterization, which we restrict to the experimental spectrum $I_{\perp}(\nu)$.

spectrum $I_0(\nu)$ and anisotropic spectrum $I_2(\nu)$ generated, respectively, by the trace $\alpha(r)$ and anisotropy $\beta(r)$ of the CI polarizability tensor of a pair of atoms interacting at a distance r: [1]

$$\begin{pmatrix} I_{\perp}(\nu) \\ I_{//}(\nu) \end{pmatrix} = \begin{pmatrix} 1 & 7/45 \\ 0 & 2/15 \end{pmatrix} \begin{pmatrix} I_0(\nu) \\ I_2(\nu) \end{pmatrix}. \tag{7}$$

The knowledge of the depolarized and isotropic spectra allows therefore to test the models of induced polarizability and intermolecular potential of the studied gas. For a relatively heavy atom such as xenon, a semiclassical approximation with quantum corrections may suffice to calculate its depolarized spectrum $I_{\perp}(\nu)$ and its isotropic spectrum $I_0(\nu)$, at least over the spectral width that has been experimentally explored to date (less than ν=130 cm^{-1} in this case [2-5]). Here, we applied the same semi-classical method as the one already successfully used for rare gas mixtures such as Ne-Ar or Kr-Xe [60] or more recently for pure krypton [11]. To summarize what we have described in detail in these papers, we have first calculated the depolarized and isotropic classical spectra $I^{cl}(\nu)$ from the calculation of atomic trajectories for a pair of atoms. For each spectrum, we then distinguished two contributions: that of the pairs of bound or metastable atoms (BM), trapped in the well of the effective interatomic potential (about one third of the depolarized integrated intensity and between 33% and 40% in the isotropic case for xenon at 295 K), and those of the pairs of free atoms (FR) circulating between infinity and the effective potential barrier. At this stage of the calculation, the moments (necessarily even) of a classical spectrum must be equal to the corresponding moments K_{2n} calculated by using the sum rule for n=0, 1 and 2 [11]:

$$K_{2n} = 2k_0^{-4} \int_0^{\infty} I^{cl}(\nu) \left(2\pi\nu\right)^{2n} d\nu \tag{8}$$

To obtain the semiclassical spectra of Xenon, we multiplied $I^{cl}(\nu)$ by a desymmetrization function $D(\nu)=(1+\delta\Lambda(\nu))\exp(2\pi\nu\tau_0)$, where $\tau_0=\hbar/2k_BT$ and $\delta\Lambda(\nu)$ is an even function of quantum origin specific to the studied spectrum. On the one hand, these semiclassical spectra necessarily respect the detailed balance principle, $I(\nu)=I(-\nu)\exp(4\pi\nu\tau_0)$. On the other hand, according to our method described in our previous paper [11], the $\delta\Lambda(\nu)$ function is fitted so that

$$\delta K_{2n} = 2k_0^{-4} \int_0^{\infty} \delta\Lambda(\nu)\, I^{cl}(\nu) \cosh\left(2\pi\nu\tau_0\right) \left(2\pi\nu\right)^{2n} d\nu \tag{9}$$

where δK_{2n} stands for the Wigner-Kirkwood quantum correction [61] of the classical spectral moment K_{2n}. As a final check, the successive semiclassical moments

$$M_n = k_0^{-4} \int_{-\infty}^{\infty} I(\nu) \left(2\pi\nu\right)^{2n} d\nu \tag{10}$$

must be close to those deduced from the classical moments, their Wigner-Kirkwood corrections and their dynamical quantum corrections ($\tau_0^2 K_{2n}$ divided by 2 or 6) calculated by using the sum rule: [11]

$$\begin{cases} M_{2n} \underset{n\geq 0}{=} \mathrm{K}_{2n} + \delta\mathrm{K}_{2n} + \dfrac{\tau_0^2}{2}\mathrm{K}_{2n+2} \\ M_{2n-1} \underset{n\geq 1}{=} \tau_0 \left(\mathrm{K}_{2n} + \delta\mathrm{K}_{2n} + \dfrac{\tau_0^2}{6}\mathrm{K}_{2n+2} \right) \end{cases} \tag{11}$$

In the case of Xenon, the dynamical quantum and Wigner-Kirkwood corrections are very small, almost negligible for M_0 and M_2, and of the order of a percent for M_4. Furthermore, the moments calculated from the computed spectra match the moments calculated by the sum rule to within 1%.

3.2. Depolarized spectrum: results and analysis

The depolarized spectrum of xenon at 294.5 K is shown in Figs. 2-4. On these figures, the experimental values determined by Dixneuf, Chrysos and Rachet (DCR) [4] are reported. The experimental values of Zoppi et al [3] and of Profitt, Keto and Frommhold (PKF) [2] are not reported since they are very close to the previous ones and can hardly be distinguished from them on a logarithmic scale. In the same figures, theoretical depolarized spectra are reported by using three potentials: the "universal" potential (UP) defined in Ref. [8] and used by DCR, and the BFW and MTT potentials presented in this work. Intensities generated by the MP2 and B3LYP anisotropies calculated ab initio by Maroulis et al. [6] are presented in Fig. 2 and 3, respectively. The UP/MP2 spectrum is very close to the one calculated by DCR using quantum methods, which confirms partly the relevance of our semiclassical method. Nevertheless, our UP/B3LYP intensities diverge by higher values from DCR calculations beyond 100 cm^{-1}. In Fig. 2, compared to the experimental measurements, a lack of intensity is noticeable below 70 cm^{-1} for the MP2 model regardless of the potential, while the agreement is satisfactory for higher frequencies. The result is the opposite in Fig. 3 for the B3LYP model, which generates intensities close to the experiment at low frequencies but generates too high intensities above 70 cm^{-1}. In Fig. 4, intensities correspond to our analytical model of polarizability, hereafter referred to as the parameterized model (PM),

$$\beta(r) = \frac{6\alpha_0^2}{r^3} + \left(6\alpha_0^3 + \frac{\gamma C_6}{3\alpha_0} \right) \frac{1}{r^6} + \frac{24\alpha_0^2 C}{r^8} - g_2 \exp\left(-\frac{r-\sigma}{r_{21}} - \left(\frac{r-\sigma}{r_{22}} \right)^2 \right), \tag{12}$$

where, $\alpha_0 = 28.44\ e^2 a_0^2 E_h^{-1}$, $\gamma = 8605\ e^4 a_0^4 E_h^{-3}$ and $C = 233.47\ e^2 a_0^4 E_h^{-1}$ stand for atomic polarizability, hyperpolarizability and quadrupole polarizability, respectively (B3LYP [6]), $C_6 = 285.9$ au (DOSD [56]) for the dispersion force coefficient, and $\sigma = 7.389$ bohrs for the xenon diameter. Besides, $g_2 = 2{,}159$ au, $r_{21} = 0{,}655$ bohrs and $r_{22} = 1.890$ bohrs are fitted parameters obtained according the analysis of CILS spectral moments described in Ref.[11]. In this PM case, based on often used empirical models [2, 62, 63], the agreement with the experiment is very good at low frequencies while a slight deficit in intensity appears at higher frequencies. For MP2 and PM models, the BFW potential generates higher intensities at high frequencies and appears to respond best to the experimental data.

In Table 3, we report the values of the spectral moments M_n (n=1 to 4) that can be deduced from the theoretical spectra for the three potentials considered (BFW, MTT, UP), two quantum models of polarizability calculated by Maroulis (MP2, B3LYP) [6] and our parametrized model (PM). We also report the values of the moments that can be deduced from DCR experimental data [4]. Since these experimental intensities could only be measured from 4 cm^{-1}, due to the presence of the Rayleigh line, we had to extrapolate the values of the successive experimental moments in the interval [0, 4] cm^{-1}. To do this, we based ourselves on the observation that, whatever the polarizability model and the potential considered, the theoretical contribution of this interval is about 53% for M_0, 4.3% for M_1 and M_2, 0.63‰ for M_3 and M_4. Besides in figure 5, it is possible to visualize the ratios M_n^{calc}/M_n^{exp} between the successive calculated and experimental spectral moments. We also considered the lower and upper limits of the ratios between theoretical and experimental moments by taking into account the uncertainty bars of the experimental measurements. The MP2 model of anisotropy [6] fails to fall within the limits set by the uncertainty bars because of the too low intensities it generates at low frequencies. The MP2 depolarized intensities are close to experiment beyond 70 cm^{-1} but it is not sufficient to get moment values compatible with those inferred from experiment (even for M_3 and M_4 because the interval [70, ∞[cm^{-1} contributes only about one-fifth of these high-order moments). The spectral moments associated with the B3LYP model are within the uncertainty bars, but with values of M_3 and M_4 close to the upper limit (this time, the frequency range beyond 70 cm^{-1} where the values of the B3LYP intensities exceed the experimental intensities contributes 30%). From the analysis of Table 3 and Fig.4, it appears that the PM model is the one that, whatever the chosen potential, is fully compatible with the experimental measurements of the spectral moments. Indeed, this is a logical consequence of the way this analytical model was developed, based on the analysis of spectral moments.

Table 3: Experimental and computed spectral moments of the depolarized CILS spectrum of Xenon. Experimental moments are extrapolated from the experimental intensities published by DCR [4]. Three potentials (BFW, MTT, UP [8]) and three anisotropy models (PM, B3LYP [6], MP2 [6]) are considered.

	Mini	Experiment	Maxi	PM/BFW	PM/MTT	PM/UP	units
M_0	1345	1512	1679	1497.1	1497.1	1550.7	$Å^9$
M_1	3.529	3.982	4.436	4.051	4.103	4.249	10^{13} $Å^9$ s^{-1}
M_2	2.529	3.080	3.431	3.133	3.173	3.286	10^{27} $Å^9$ s^{-2}
M_3	7.538	8.597	9.656	8.528	8.507	8.565	10^{38} $Å^9$ s^{-3}
M_4	5.861	6.684	7.508	6.619	6.603	6.650	10^{52} $Å^9$ s^{-4}
	B3LYP/BFW	B3LYP/MTT	B3LYP/UP	MP2/BFW	MP2/MTT	MP2/UP	units
M_0	1429.5	1429.5	1478.2	1246.3	1246.3	1289.0	$Å^9$
M_1	3.634	3.647	3.823	3.203	3.204	3.340	10^{13} $Å^9$ s^{-1}
M_2	2.811	2.821	2.957	2.477	2.478	2.583	10^{27} $Å^9$ s^{-2}
M_3	9.169	9.025	9.624	7.349	7.238	7.451	10^{38} $Å^9$ s^{-3}
M_4	7.153	7.037	7.503	5.717	5.629	5.795	10^{52} $Å^9$ s^{-4}

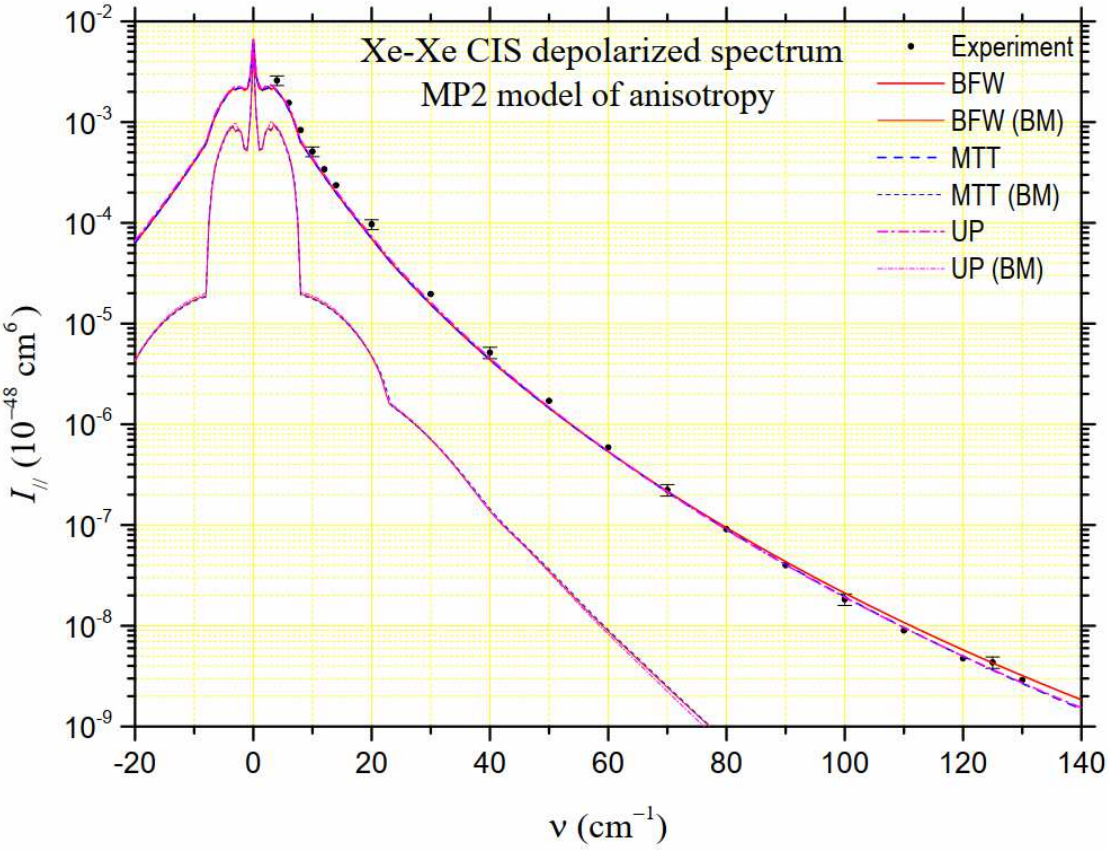

Fig.2. Comparison between the calculated depolarized CILS spectra of Xe_2 at T=294.5 K using different interatomic potentials (BFW: red; MTT: blue; UP: indigo) and *ab initio* MP2 pair polarizability anisotropy of Maroulis [6] with the experimental measurements of Ref.[4]. The bound and metastable pair contributions are represented by dashed lines.

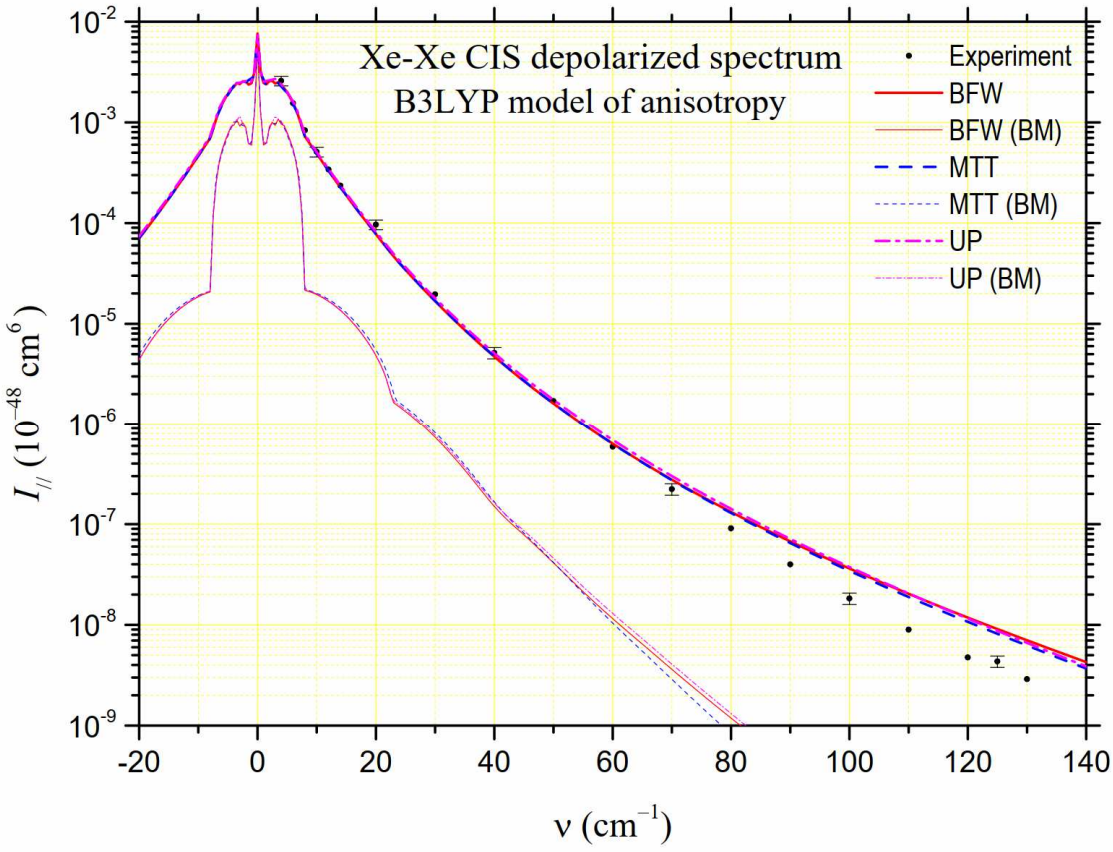

Fig. 3. The same comparison as in Figure 2 between depolarized spectra generated by three potentials but for the B3LYP pair polarizability anisotropy.

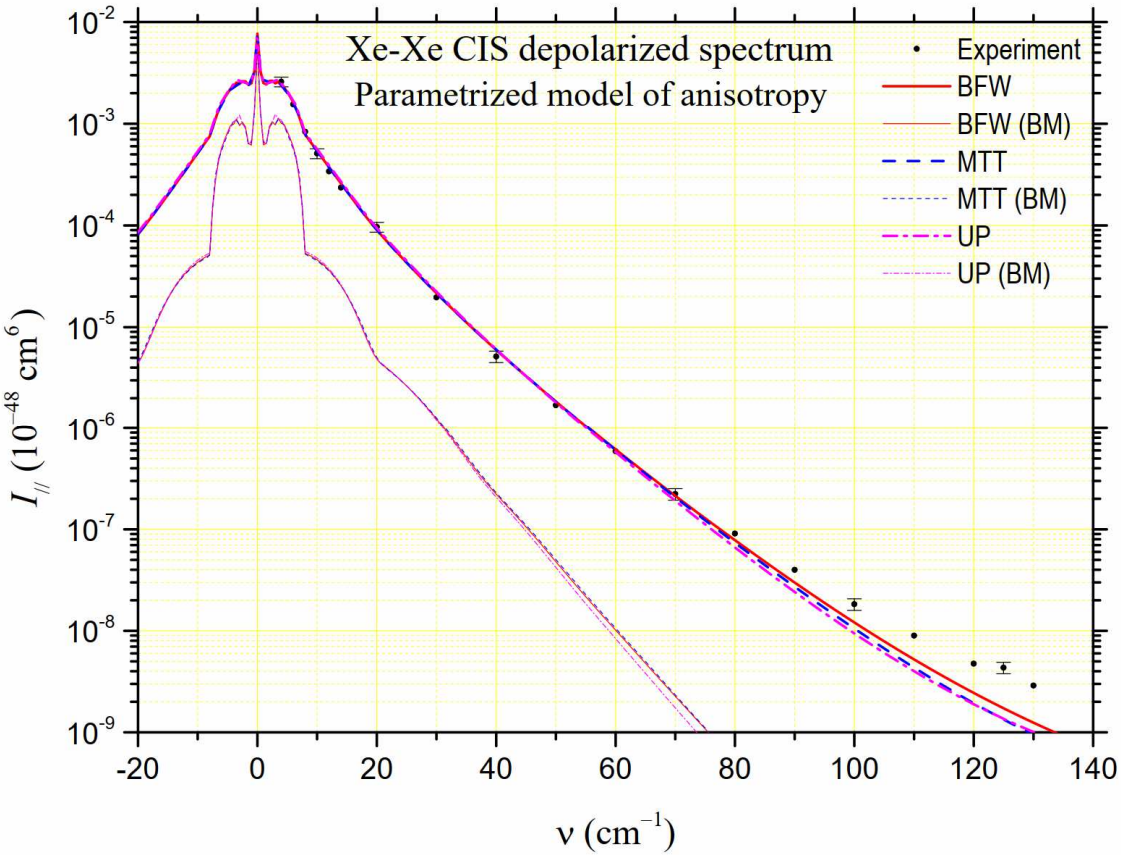

Fig. 4. The same comparison as in Figure 2 between depolarized spectra generated by three potentials but for the PM pair polarizability anisotropy.

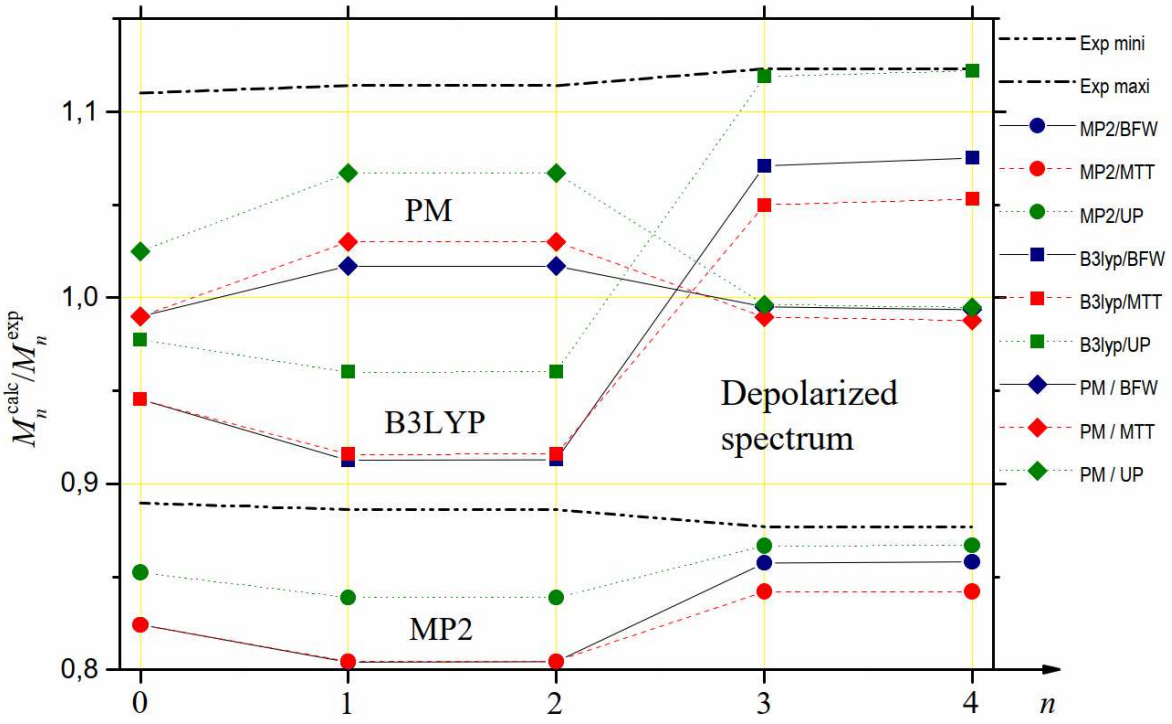

Fig.5. Ratios M_n^{calc}/M_n^{exp} of the calculated moments of the depolarized spectrum to the experimental ones extrapolated from Ref.[4]. Calculations were performed using BFW (blue), MTT (red) and UP (green) interatomic potentials for the three models of anisotropy studied: MP2 (●), B3LYP (■) and PM (◆). The upper and lower limit values of the ratios defined by the experimental uncertainty bars are drawn in dash-dot or dash-dot-dot black lines, respectively.

3.3. Isotropic spectrum: Results and analysis

The analysis of the isotropic spectrum is much more delicate. Experimentally, two series of measurements are available, performed by PKF [2] and more recently by Chrysos and Rachet (CR) [5]. Given the uncertainty bars, these series are compatible. However, uncertainties are very large. This is because the spectrum is deduced, according to Eq.(7), from the subtraction of two quantities,

$$I_0(\nu) = I_\perp(\nu) - \tfrac{7}{6} I_{//}(\nu)\,, \tag{13}$$

that are generally close together. The isotropic intensities $I_0(\nu)$ are of the order of a few percent of $I_\perp(\nu)$ at lower frequencies even if they can reach a few tenths at the highest frequencies. Moreover, the presence of the Rayleigh line and its wings makes it particularly difficult to determine $I_\perp(\nu)$ at low frequencies (and also the depolarized spectrum $I_{//}(\nu)$ at $\nu\approx 0$). Thus, PKF's isotropic spectrum measurements only start at 23 cm^{-1}. Even more revealing of the experimental difficulties in extracting the isotropic spectrum from the polarized and depolarized spectra, these of Chrysos and Rachet start at 70 cm^{-1}. We report both series of intensities in Figs. 6-8. The experimental spectrum appears to be divided into two parts. Up to about 35 cm^{-1}, the intensity decreases strongly in an almost exponential way. Beyond, the decrease is less strong while gradually stronger. The large dispersion of the experimental data can be noticed in the latter frequency range, in accordance with the big size of the uncertainty bars. For this reason, using the least squares method, we calculated "average" experimental intensities by degree 2 polynomial fitting of the logarithms of all the experimental intensities (these of PKF and these of CR) from 35 cm^{-1} to 130 cm^{-1}. The "synthesis" curve thus obtained is represented by a black dotted line in Figs 6-8. In Fig.6 and 7, we also present the theoretical intensities generated by the MP2 and B3LYP models of trace of Maroulis [6] for the three potentials considered in this work (BFW, MTT, UP [8]). In Fig.8, we present similarly the theoretical isotropic spectrum generated by the PM trace,

$$\alpha(r) = \left(4\alpha_0^3 + \frac{5\gamma C_6}{9\alpha_0}\right)\frac{1}{r^6} + \frac{20\alpha_0^2 C}{r^8} - g_0 \exp\left(-\frac{r-\sigma}{r_{01}} - \left(\frac{r-\sigma}{r_{02}}\right)^2\right), \tag{14}$$

where $g_0 = 1.275$ au, $r_{01} = 0{,}49$ bohrs and $r_{02} = 2.958$ bohrs are fitted parameters deduced from the method presented in Ref.[11], as for the PM anisotropy. From the analysis of the figures, it appears that the model that comes closest to the "synthesis" curve is the PM model for MTT or BFW potentials. However, regardless of the potential, both MP2 and B3LYP models are fully consistent with the experimental data in the 35-130 cm^{-1} frequency range. Below 35 cm^{-1}, PKF's measurements need to be confirmed, given the uncertainties in measuring the polarized spectrum at low frequencies. The quasi-exponential growth in intensity as the frequency shift tends to zero is nevertheless found with the MP2, B3LYP and PM models, albeit at lower frequencies.

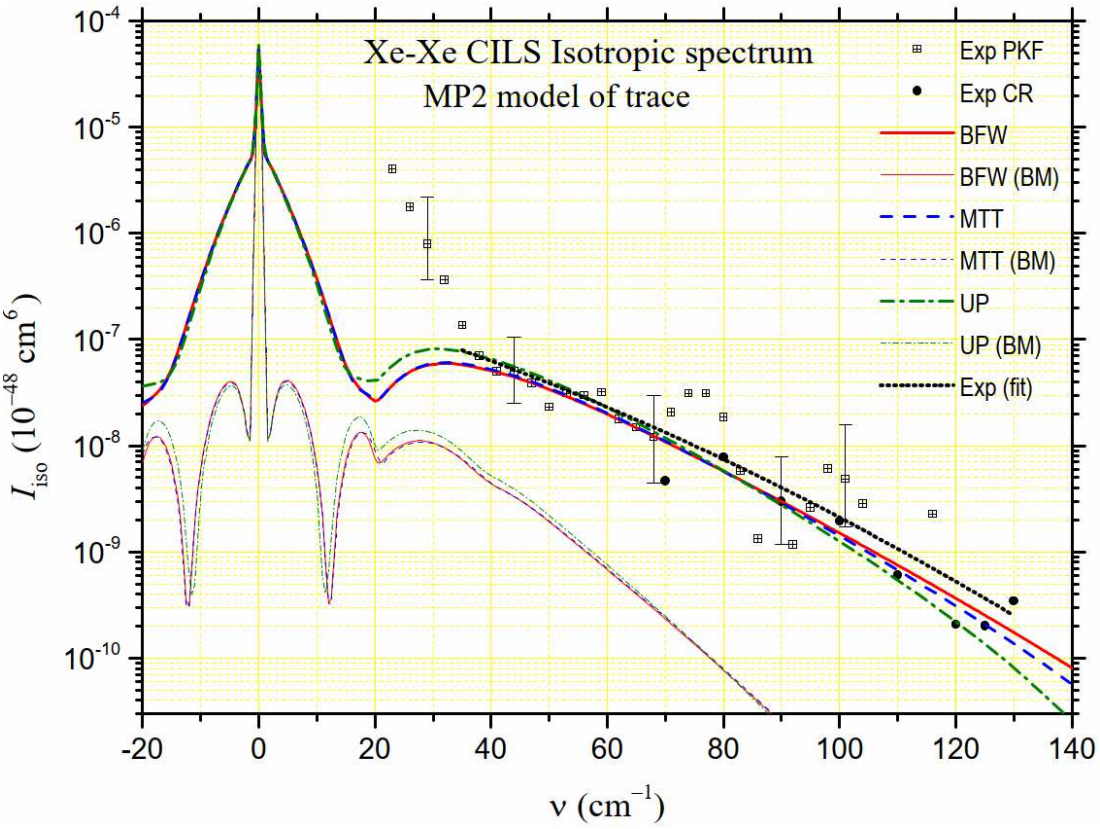

Fig.6. Comparison between the calculated isotropic CILS spectra of Xe_2 at T=294.5 K using different interatomic potentials (BFW: red; MTT: blue; UP: indigo) and *ab initio* MP2 pair polarizability anisotropy of Maroulis [6] with the experimental measurements of Ref.[2, 5]. The bound and metastable pair contributions are represented by dashed lines and the curve making the "synthesis" of all the experimental data between 35 cm^{-1} and 130 cm^{-1} by black dots.

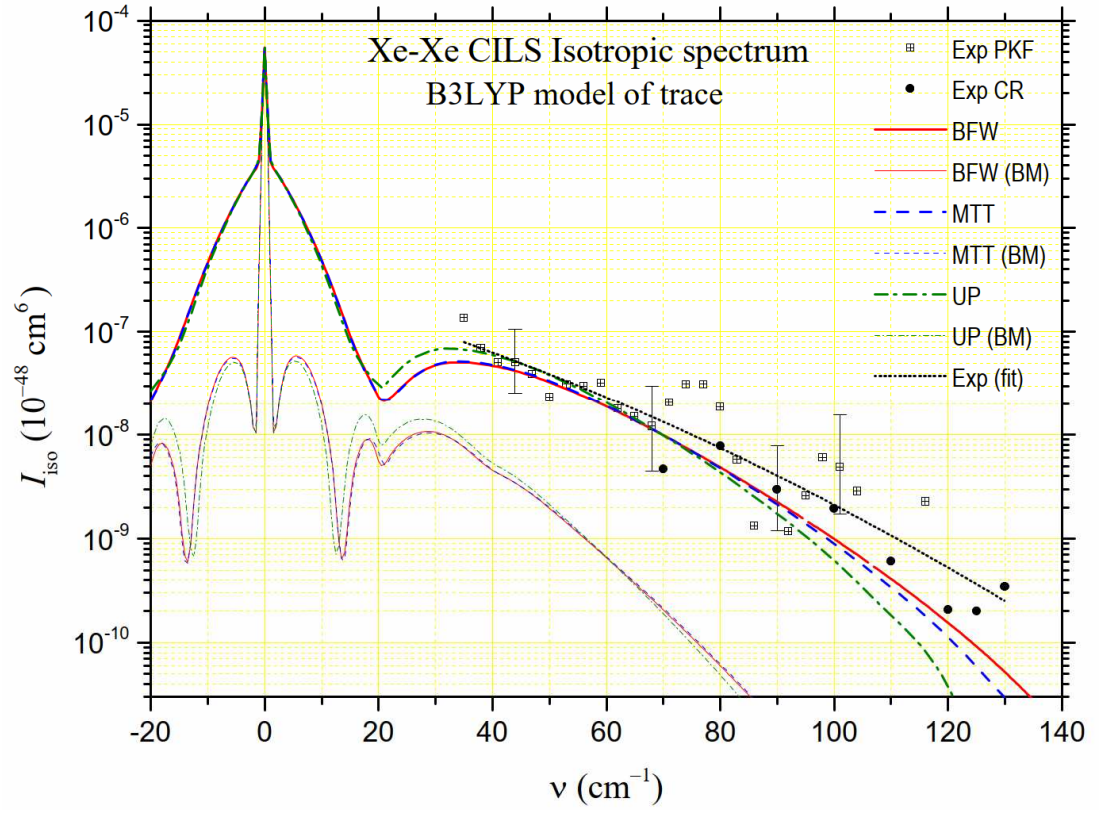

Fig. 7. The same comparison as in Figure 6 between isotropic spectra generated by three potentials but for the B3LYP pair polarizability anisotropy computed by Maroulis [6].

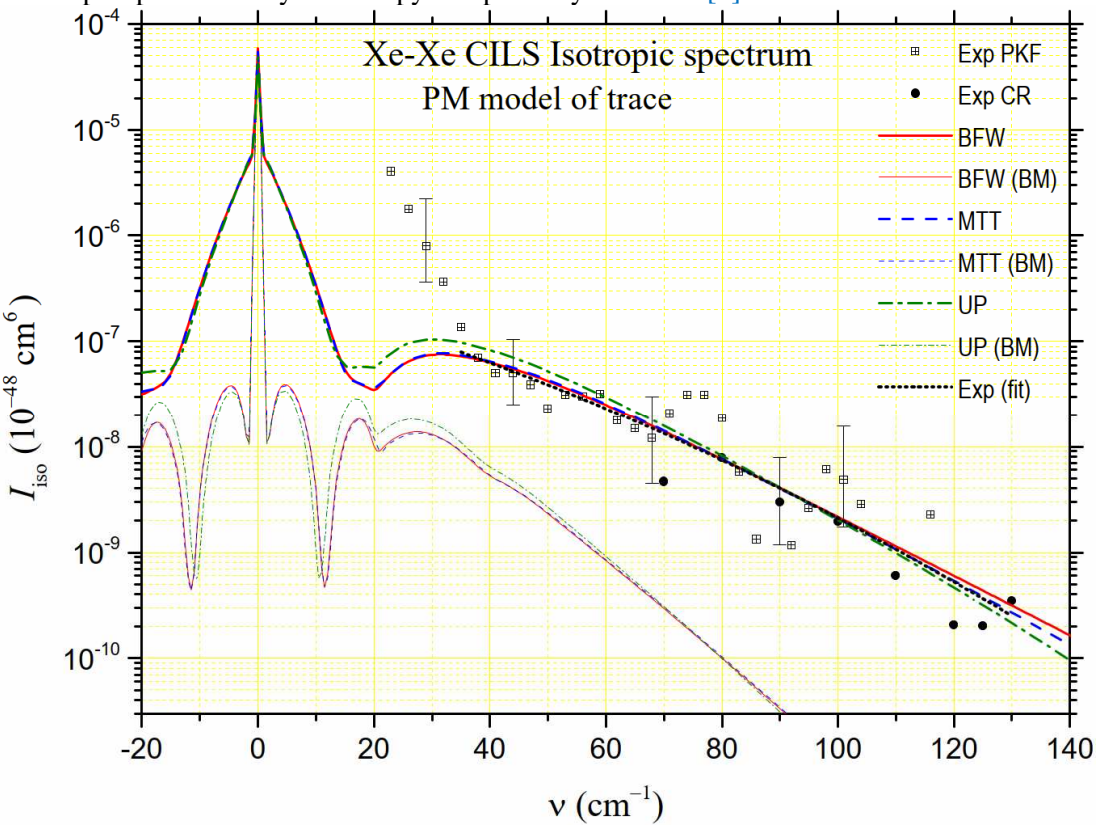

Fig. 8. The same comparison as in Figure 6 between isotropic spectra generated by three potentials but for the PM pair polarizability anisotropy proposed in this work.

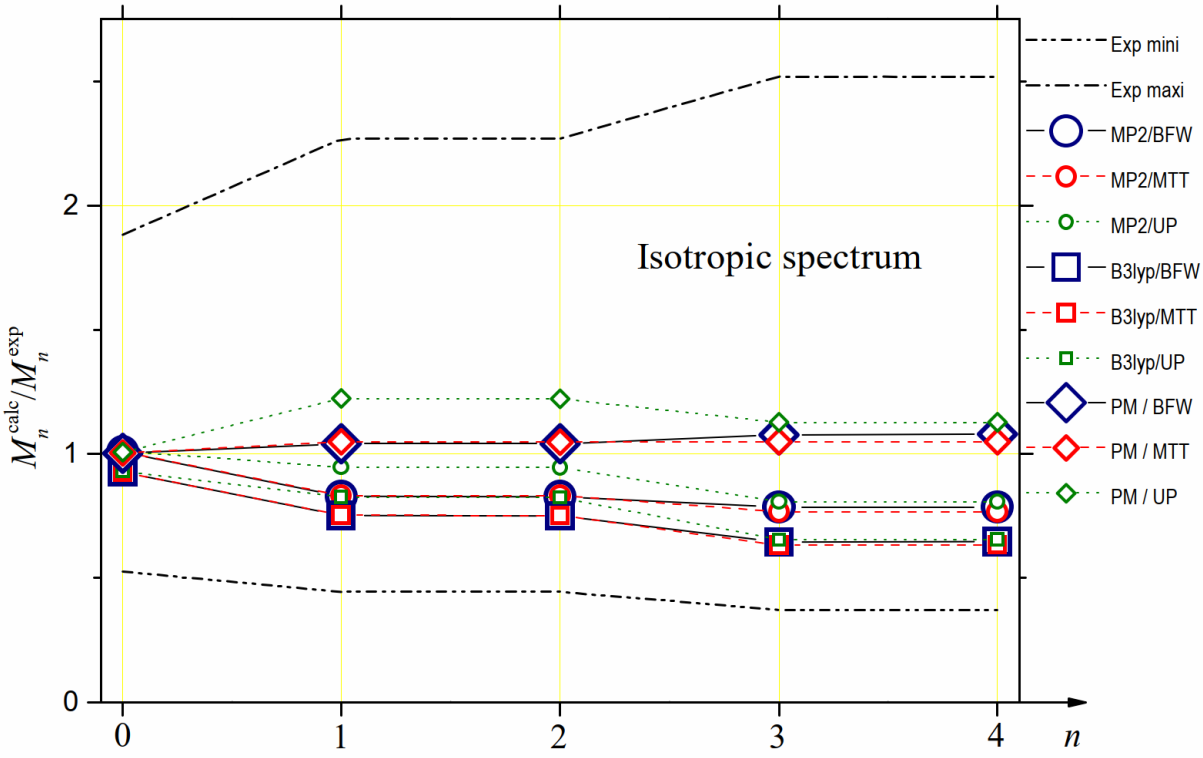

Fig.9. Ratios M_n^{calc}/M_n^{exp} of the calculated moments of the isotropic spectrum to the experimental ones extrapolated from Refs.[2, 5]. Calculations were performed using BFW (blue), MTT (red) and UP (green) interatomic potentials for the three models of trace studied: MP2 (○), B3LYP (□) and PM (◇). Extrapolated from the experimental uncertainty bars, the upper and lower limit values of the ratios are drawn in dash-dot and dash-dot-dot black lines, respectively.

The study of the spectral moments confirms the previous considerations, albeit in a more uncertain way. The spectral range inaccessible to the experiment is much larger than in the case of the depolarized spectrum. The contribution to the spectral moments of the interval [0, 35] cm^{-1} cannot be determined from experimental measurements while it is decisive for the value of M_0. However, Fig.8 highlights a very good agreement between the isotropic intensities generated by the PM model (and, to a lesser extent, by the MP2 model) for BFW or MTT potentials and the "synthesis" curve of the experimental measurements of PKF and CR beyond 35 cm^{-1}. This observation led us to hypothesize that it is possible to extrapolate the relative contributions of the interval [0, 35] cm^{-1} to experimental moments from the contributions of the same interval for the PM model and both BFW and MTT potentials: ≈96,6% for M_0, ≈0.22% for M_1 and M_2, ≈0.03% for M_3 and M_4 (MP2 model gives similar results). Based on this assumption, the experimental spectral moments are listed in Table 4 next to the calculated moments for the three models MP2, B3LYP and PM and the three potentials BFW, MTT and UP. The ratios M_n^{calc}/M_n^{exp} between the successive calculated and experimental spectral moments are given in Fig.9. This figure confirms that the three trace models studied are compatible with the experiment given the very large uncertainty bars. Of course, and this is the effect of the previously described hypothesis for the interval [0, 35] cm^{-1}, we find M_0^{calc}/M_0^{exp}≈1 for the PM model of trace whatever the potential is, but it is also checked for the MP2 model and to a lesser extent for the B3LYP model. For the higher order moments, to which the interval [0, 35] cm^{-1} contributes little, it is the PM model of the trace that appears to be in best agreement with the experimental measurements, both for the BFW potential and the MTT potential.

Table 4: Experimental and computed spectral moments of the isotropic CILS spectrum of Xenon. Experimental moments are extrapolated from the experimental intensities published by PKF [2] and CR [5]. Three potentials (BFW, MTT, UP [8]) and three anisotropy models (PM, B3LYP [6], MP2 [6]) are considered.

	Mini	Experiment	Maxi	PM/BFW	PM/MTT	PM/UP	units
M_0	0.202	0.385	0.725	0.385	0.386	0.387	$Å^9$
M_1	0.98	2.21	5.00	2.29	2.30	2.69	$10^{10}\ Å^9\ s^{-1}$
M_2	0.76	1.72	3.89	1.78	1.80	2.09	$10^{24}\ Å^9\ s^{-2}$
M_3	1.05	2.84	7.14	3.05	2.97	3.19	$10^{36}\ Å^9\ s^{-3}$
M_4	0.82	2.22	5.59	2.39	2.32	2.50	$10^{50}\ Å^9\ s^{-4}$
	B3LYP/BFW	B3LYP/MTT	B3LYP/UP	MP2/BFW	MP2/MTT	MP2/UP	units
M_0	0.356	0.357	0.357	0.387	0.387	0.388	$Å^9$
M_1	1.66	1.66	1.82	1.83	1.83	2.09	$10^{10}\ Å^9\ s^{-1}$
M_2	1.29	1.29	1.41	1.42	1.43	1.62	$10^{24}\ Å^9\ s^{-2}$
M_3	1.83	1.79	1.86	2.22	2.17	2.29	$10^{36}\ Å^9\ s^{-3}$
M_4	1.43	1.41	1.46	1.74	1.70	1.79	$10^{50}\ Å^9\ s^{-4}$

4. Conclusion

In this paper, we applied the methods we developed in previous papers [9-11, 60] to determine the potential and polarizability of xenon from the available experimental data. The BFW and MTT potentials thus defined and the parametrized model of the anisotropy and trace of the polarizability tensor of Xenon allowed us to calculate its depolarized and isotropic CIS spectra. The comparison of these theoretical spectra with the experimental spectra measured by several groups [2-5] confirms the validity of our approach. In particular in the case of the isotropic CIS spectrum, it is remarkable that the theoretical spectrum deduced from our models coincides quite exactly with a polynomial fit of degree 2 of the logarithms of all experimental intensities in the interval [0, 35] cm^{-1}. Indeed, both the BFW and MTT potentials and the trace and anisotropy analytical models (PM) presented in this work are able to account for the available experiments.

References

1. L. Frommhold, *Collision-induced scattering of light and the diatom polarizabilities*, Adv. Chem. Phys. **46**, 1 (1981).
2. M. H. Proffitt, J. W. Keto, and L. Frommhold, Can. J. Phys. **59**, 1459 (1981).
3. M. Zoppi, M. Moraldi, F. Barocchi, R. Magli, and U. Bafile, Chem. Phys. Lett. **83**, 294 (1981)
4. S. Dixneuf, M. Chrysos and F. Rachet. *Anisotropic collision-induced Raman scattering by the Kr-Xe gas mixture*, J. Chem. Phys. **131**: 074304 (2009).
5. M. Chrysos and F. Rachet, *Heavy rare-gas atomic pairs and the "double penalty"issue: isotropic Raman lineshapes by Kr_2, Xe_2, and KrXe at room temperature*. J. Chem. Phys.**143**:174301 (2015).
6. G. Maroulis, A. Haskopoulos and D. Xenides, Chem. Phys. Lett. **396**: 59 (2004).
7. J. J. H. van den Biesen, F. A. Stockvis, E. H. van Veen, and C. J. N. van den Meijdenberg, Physica A (Amsterdam), 100, 375 (1980)
8. A. D. Koutselos, E. A. Mason and L. A. Viehland, J. Chem. Phys. **93**, 7125 (1990)
9. M. S. A. El-Kader and B. M. Taher, Z. Phys. Chem., **217**: 1127 (2003).
10. M. S. A. El-Kader , A. A. El-Sadek, B. M. Taher and G. Maroulis, Mol. Phys., **109**: 1677 (2011).
11. J.-L. Godet and M. S. A. El-Kader, *Isotropic and anisotropic collision-induced light scattering spectra of krypton gas simultaneously fitted by ground state interatomic potential*, J. of Quant. Spectr. & Rad. Transf. **288**: 108251 (2022)
12. G. C. Maitland, M. Rigby, E. B. Smith and W. A. Wakeham. Intermolecular forces – their origin and determination. Clarendon, Oxford (1981).
13. G. C. Maitland and W. A. Wakeham. Mol. Phys. **35**:1443 (1978).
14. E. R. Cohen and G. Birnbaum, J. Chem. Phys. **62**:3807 (1975).
15. X. Sheng, H. Zhu, Z. Zhang, D. Zhang, J. Lu and J. Xiao, Int. J. Quant. Chem.**119**: e25800 (2019).
16. J. C. Xie, T. Kar and R. H. Xie, Chem. Phys. Lett. **591**: 69(2014).
17. R. Hellmann, B. Jäger and E. Bich, J. Chem. Phys., **147**: 034304 (2017).
18. R. A. Aziz and M. J. Slaman, Mol.Phys., **57**: 825 (1986).
19. A. K. Dham, W. J. Meath, A. R. Allnatt, R. A. Aziz, and M. J. Slaman, Chem. Phys. **142**: 173 (1990).
20. P. Slavíček, R. Kalus, P. Paška, I. Odvárková, P. Hobza, and A. Malijevský, J. Chem. Phys. **119**: 2102 (2003).
21. M. Hanni, P. Lantto, N. Runeberg, J. Jokisaari, and J. Vaara, J. Chem. Phys. **121**: 5908 (2004).

22. D. E. Freeman, K. Yoshino, and Y. Tanaka, J. Chem. Phys. **61**, 4880 (1974).
23. J. H. Dymond, K. N. Marsh, R. C. Wilhoit and K. C. Wong, Virial coefficients of pure gases and mixtures, Edited by M. Frenkel and K.N. Marsh, Landolt-Bornstein - Group IV Physical Chemistry, 21, Subvolume A "*Virial Coefficients of Pure Gases*" Springer-Verlag, Heidelberg (2002).
24. C. A. Pollard; Ph.D. Thesis, Univ. London, London, England, (1971).
25. J. Brewer, Technical Report No. 67–2795, AFOSR (1967).
26. R. Hahn, K. Schaefer, B. Schramm, Ber. Bunsen-Ges. Phys. Chem. **78**: 287 (1974).
27. H. Schmiedel, R. Gehrmann, B. Schramm, Ber. Bunsen-Ges. Phys. Chem. **84**: 721 (1980).
28. B. Schramm, W. Mueller, Ber. Bunsen-Ges. Phys. Chem. **86:** 110 (1982).
29. B. Schramm, H. Schmiedel, R. Gehrmann, R. Bartl, Ber. Bunsen-Ges. Phys. Chem. **81**: 316 (1977)
30. A. Michels, T. Wassenaar, and P. Louwerse, Physica **20**: 99 (1954).
31. C. G. Reeves, R. Whytlaw-Gray, Proc. R. Soc. London, A. **232:** 173 (1955)
32. E. Whalley, Y. Lupien, and W. G. Schneider, Can. J. Chem. **33**: 633 (1955).
33. J. A. Beattie, R. J. Barriault, and J. S. Brierley, J. Chem. Phys. **19**: 1222 (1951).
34. S. Perez, H. Schmiedel, B. Schramm, Z. Phys. Chem. (Munich). **123**: 35 (1980).
35. H.-P. Rentschler and B. Schramm, Ber. Bunsenges. Phys. Chem. **81**: 319 (1977).
36. A. G. Clarke and E. B. Smith, J. Chem. Phys. **48**: 3988 (1968).
37. R. A. Dawe and E. B. Smith, J. Chem. Phys. **52**: 693 (1970).
38. M. Goldblatt and W. E. Wageman, Phys. Fluids **14**: 1024 (1971).
39. E. F. May, R. F. Berg, and M. R. Moldover, Int. J. Thermophys. **28**: 1085(2007).
40. H. Lin, J. Che, J. T. Zhang, and X. J. Feng, Fluid Phase Equilib. **418**: 198(2016).
41. E. Vogel, Int. J. Thermophys. **37**: 63 (2016).
42. B. N. Srivastava and A. K. Barua, J. Chem. Phys. **32**: 427 (1960).
43. S. C. Saxena and F. E. Davis, J. Phys. E **4**: 681 (1971).
44. N. B. Vargaftik and L. V. Yakush, J. Eng. Phys. **21**: 1156 (1971).
45. G. S. Springer and E. W. Wingeier, J. Chem. Phys. **59**: 2747 (1973).
46. A. G. Shashkov, N. A. Nesterov, V. M. Sudnik, and V. I. Aleinikova, J. Eng.Phys. **30**: 439 (1976).
47. J. Kestin, R. Paul, A. A. Clifford, and W. A.Wakeham, Physica A **100**: 349(1980).
48. M. J. Assael, M. Dix, A. Lucas, and W. A.Wakeham, J. Chem. Soc., FaradayTrans. 1 **77**: 439 (1981).
49. B. Le Neindre, Y. Garrabos and R. Tufeu, Physica A **156**: 512(1989).

50. S. Visner, in "Proceedings of the American Physical Society," Phys. Rev. **82**: 291 (1951).

51. I. Amdur and T. F. Schatzki, J. Chem. Phys. **27**: 1049 (1957).

52. J. Kestin, K. Knierim, E. A. Mason, B. Najafi, S. T. Ro, and M. Waldman, J. of Phys. and Chem. Ref. Data, **13**: 223, (1984).

53. J. A. Barker, R. A. Fisher and R. O. Watts, Mol. Phys., **21**: 657 (1971).

54. J. F. Peng, P. Li, J. Ren, L. W. Qiao and K. T. Tang, J. At. Mol. Sci., **2**: 289, (2011).

55. K. T. Tang and J. P. Toennies, J. Chem. Phys. **80**: 3726, (1984).

56. A. J. Thakkar, H. Hetterna, and P. E. S. Wormer, J. Chem. Phys. **97**: 3252 (1992).

57. E. Bich, R. Hellmann and E. Vogel, Mol. Phys.,**106**: 1107 (2008).

58. L. Monchick, K. S. Yun and E. A. Mason, J. Chem. Phys.**39**: 654, (1963).

59. A. Elliasmine, J.-L.Godet and Y. Le Duff, Mol. Phys. **90**(2), 147 (1997).

60. J.-L. Godet and M. S. A. El-Kader, *Collision-induced light scattering (CILS) and collision-induced absorption (CIA) spectra for monatomic rare gas mixtures*, J. of Quant. Spectr. & Rad. Transf. **231**: 9 (2019)

61. R. W. Hartye, C. G. Gray, J. D. Poll and M. S. Miller, Mol. Phys. **29**, 825 (1972).

62. N. Meinander, G. C. Tabisz and M. Zoppi, J. Chem. Phys. **84**, 3005 (1986).

63. S. M. El-Sheikh, G. C. Tabisz and A. D. Buckingham, Chem. Phys., **247**: 407 (1999).